HiSST: 3rd International Conference on
High-Speed Vehicle Science & Technology

14–19 April 2024, Busan, Korea

Feasibility Study of an Electric Supersonic Propeller

Jens Kunze[1], *Allan Paull*[2]

Abstract

An analysis of a supersonic propeller driven by an electric motor is performed. Recent and continuing progress in electric energy storage systems and electric motors as well as materials have opened up the design space for a large number of applications. So, too, for electrically powered flight. A propeller is the simplest method of converting electric energy into aerodynamic thrust. The analysis in this study is aimed at evaluating the predictive performance of a two dimensional and a quasi three dimensional model compared to fully three dimensional simulation results using computational fluid dynamics. Power efficiencies are calculated for a number of different propeller blades. The geometric features of particular interest are the shape of the leading and trailing edges, the thickness of the blade, its cross-sectional shape and the blade twist. The results show that, for the blades investigated here, the efficiencies predicted by the quasi three dimensional model match match the simulation results very closely for the smallest edge radius. Even the prediction by the two dimensional model is quite close to the magnitude of the blade efficiency, although it under predicts the rotational speed required to achieve it. For larger edge radii neither model makes good predictions.

Keywords: *Electric Propulsion, Supersonic Propeller*

1. Introduction

The world is electrifying. Recent reports indicate that electrification is happening across all industries [1, 2]. In part, this process is possible due to the significant advances in electric energy storage systems (EESS). However, it also creates demand for better and cheaper EESS. The specific power, i.e. power per unit mass, and specific energy, i.e. energy per unit mass, of EESS have increased to the point where more and more applications can be electrified and there is no sign of progress slowing down. Fig. 1 shows typical ranges of specific energy versus specific power for different EESS in 2011 [3]. Ten years later, commercial batteries are already achieving an order of magnitude higher specific power, albeit only for a duration of 30 s. Considering the rapid progress in EESS and the increasing demand for electrification, one can reasonably assume that even better EESS will become available in the near future.

Due to these developments, even electric supersonic propulsion becomes worth investigating. The simplest option to convert electric energy into thrust is by driving a propeller with an electric motor. Historically, propellers have only been used for subsonic flight [5]. Although attempts at using propellers for supersonic flight were made starting in the 1950s [6], they were abandoned because the problems caused by shock waves on the propeller blades could not be overcome. The turboprop driven Republic XF-84H, for instance, was renowned for technical difficulties as well as inducing severe headaches and nausea in the pilots and ground staff [7]. Hence, no attempt was made to design a propeller for the supersonic flight regime. In a recent study, sparked by the advances in EESS technology, it was demonstrated that a supersonic propeller can convert the torque delivered by a motor into thrust with efficiencies exceeding 75 % according to a simple two dimensional model [8]. The study found that reasonable efficiencies could be achieved in the Mach number range from 2 to 5.5 at 15 km to 35 km

[1] *Centre for Hypersonics, School of Mechanical and Mining Engineering, The University of Queensland, 4072 Brisbane, j.kunze@uq.edu.au*

[2] *Centre for Hypersonics, School of Mechanical and Mining Engineering, The University of Queensland, 4072 Brisbane, allan.paull@uq.edu.au*

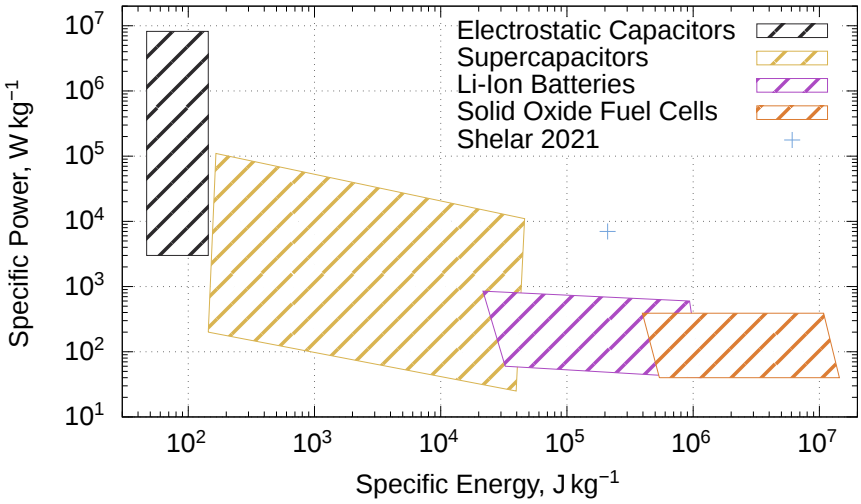

Fig 1. Typical specific power over specific energy for different electric energy storage systems in 2011, reproduced from [3], compared to a commercial lithium polymer battery in 2021 [4].

altitude. Considering the optimal shape of the supersonic propeller, a thin flat plate, it is reasonable to assume that it is difficult if not impossible to design a propeller which works well in both the subsonic and the supersonic regime, not to mention the transonic regime. This puts supersonic propellers into a similar category as supersonic combustion ramjets [9], which require a different propulsion system to get up to their minimum speed.

In this study, three dimensional computational fluid dynamics (CFD) of a propeller blade is used to evaluate the predictive capability of the model used by Kunze and Paull [8]. It is then used further to explore design aspects which can not be modelled in two dimensions, for instance the twist of the propeller blade. In Fig. 2 a simple example of a propeller driven vehicle is shown for reference. The

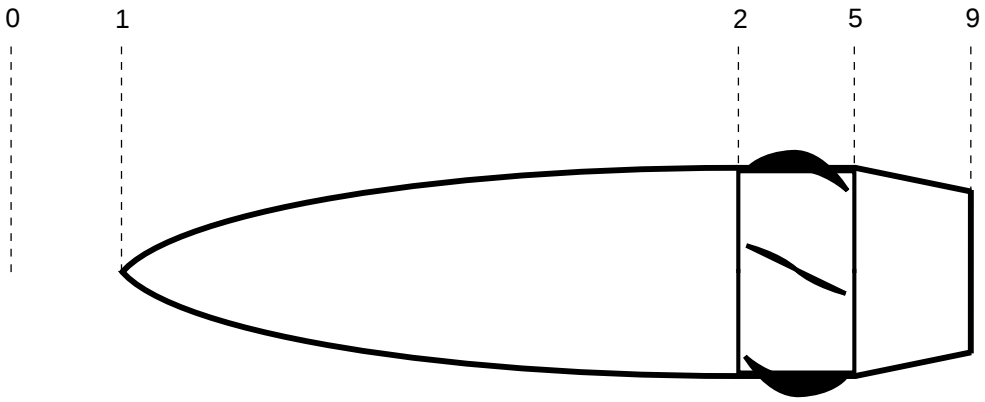

Fig 2. A sketch of a propeller driven vehicle with engine station numbering.

station numbers are shown are based on the numbering commonly used in jet engines, where 0 denotes the undisturbed freestream, 1 marks the start of the inlet, 2 is the start of the compressor, 5 denotes the end of the turbine and 9 designates the end of the engine nozzle.

2. Modelling

In this section the geometric model of the propeller blade, the flow solver and simulation setup as well as the grid convergence study are discussed. Although the focus of this study is on three dimensional blades, it is worthwhile revisiting the two dimensional flow models for understanding. Figure 3 shows a cross-section of a flat plate blade with a shock on the windward side of the blade and an expansion fan on the lee. Here, c and u denote the inflow velocity and the blade velocity respectively in a body fixed

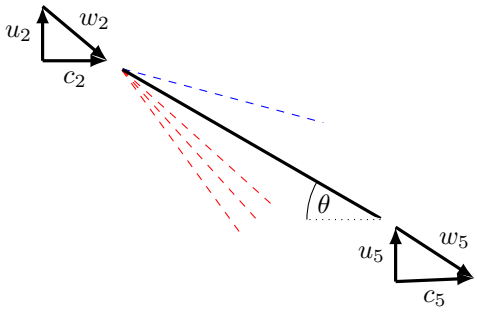

Fig 3. A sketch of a two dimensional flat plate propeller blade with velocity triangles.

coordinate system and w is the inflow velocity in a blade fixed frame of reference. The angle θ is the chord angle, i.e. the angle of the blade chord with respect to axis of rotation. If the blade rotates fast enough, i.e. if

$$u_2 > \tan(\theta) \cdot c_2 \tag{1}$$

the shock and expansion fan form as shown in Fig. 3 and the propeller can produce thrust. At lower rotational speeds the shock and expansion fan swap sides which reverses the force vector and the propeller will produce drag instead. The quantity of interest which is used as a convergence criterion and to compare the performance of different blades is the power efficiency of the blade, i.e.

$$\frac{P_T}{P_M} = \frac{c_0 F_T}{\omega M_M}, \tag{2}$$

where P_T is the thrust power and P_M is the power supplied by the electric motor. F_T designates the thrust of the blade, ω is the angular velocity of the propeller and M_M the torque required to run the propeller at ω.

2.1. Geometric Model of the Propeller Blade

The propeller blades investigated here all have the same basic dimensions: they have a chord length of 100 mm and a height of 30 mm. The chord is defined as the line connecting the centre of the leading edge to the centre of the trailing edge at a constant radius. The blade height is defined as the distance from the propeller hub to blade tip. The chord length is constant over blade height. The hub radius is 185 mm and the hub is 180 mm long.

Besides the flat plate blade shown in Fig. 3, blades with diamond cross-sections are investigated, too. One such cross-section is shown in Fig. 4 The chord of the diamond shaped blade is shown as a dashed line. The cross-section is symmetrical about the chord and is, thus, fully defined by a chord length, a chord angle and the half wedge angles φ_1 and φ_2. In the remainder of this study a diamond shaped blade with $\varphi_1 = 3°$ and $\varphi_2 = 5°$ will be referred to as a 3-5 diamond.

One key difference to the two dimensional model is that the edges on the three dimensional blade model are not perfectly sharp. Instead there are two edge types which are investigated here: round edges and flat edges. A sketch of the two shapes is shown in Fig. 5. The round edge is a circular arc which is tangent to the blade faces and the flat edge is a straight line which is perpendicular to the blade faces in the $r\varphi$-z plane of a cylindrical coordinate system where the z-axis coincides with the axis of rotation

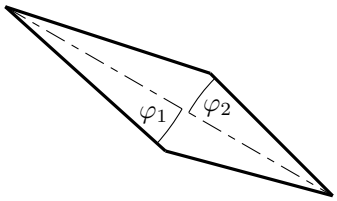

Fig 4. A sketch of a two dimensional propeller blade with a diamond shaped cross-section.

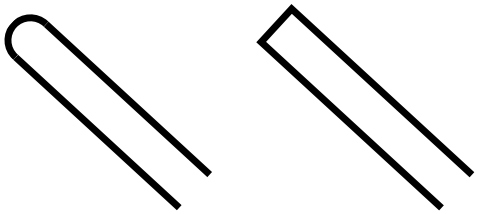

Fig 5. A sketch of the two edge shapes investigated in this study in the φr-z-plane.

of the propeller. Considering the small edge radii investigated in this study, i.e. $\leq$ 0.5 mm, it is likely that a real edge will be somewhere between round and flat due manufacturing constraints.

Another aspect that can not be modelled in two dimensions is the blade twist. The performance of the blade can be improved if the chord angle, i.e. the angle between the axis of rotation and the blade chord, varies by an appropriate amount over the blade height. Two types of blades are discussed here: one with a constant chord angle and one with a constant angle of attack over the blade height at a specified angular velocity. The angle of attack at a fixed flight condition varies with the rotational speed of the propeller. Let the local chord angle at a height h be given by

$$\alpha\left(h\right) = \tan^{-1}\left(\frac{\left(r_h + h\right)\cdot\omega}{c}\right) - \theta\left(h\right), \tag{3}$$

where ω is the angular velocity of the propeller and θ the chord angle of the blade. If the blade is twisted in such a way that the angle of attack is constant at a certain ω, it can not be constant at any other ω due to the dependence of the gradient of the first term in equation 3 with respect to h on ω. Hence, a constant angle of attack can only be achieved at a single rotational speed, i.e. if the angle of attack is constant at 2° angle of attack it will not be constant at any other angle of attack.

2.2. Computational Modelling

The software used in this study is Eilmer4 [10]. Eilmer4 is a finite-volume flow solver for the compressible Navier-Stokes equations for viscous flow. It has been developed at the University of Queensland's Centre for Hypersonics specifically for the analysis of high-speed aerothermodynamics. A rotating frame of reference mode is available for the calculation of turbomachinery flows which requires an adjustment of the equations of conservation [11]. The simulations presented here were all performed in a rotating frame of reference.

The inflow condition is uniform flow at Mach 4 and 15 km altitude, i.e. a velocity of 1180.5 m s^{-1} parallel to the axis of rotation, a pressure of 12.1 kPa and a temperature of 216.7 K. A single propeller blade and a 60° segment of the hub are modelled, hence the full propeller has six blades. Periodic boundary conditions are assigned to the side walls of the computational domain such that the conditions on the right hand side wall are equal to those on the left hand side wall but rotated by 60°. The propeller blade is modelled as an adiabatic no-slip wall and the hub surface is modelled as a free slip wall. A free slip wall forms the outer boundary of the computational domain. The simulation is run in a time accurate mode

starting from an initial condition with a velocity of 944.4 m s^{-1} parallel to the axis of rotation, a pressure of 8.5 kPa and a temperature of 216.7 K. The initial condition was chosen to reduce the time needed to reach steady state and to avoid nonphysical behaviour during the start up process.

The structured computational grids consist of 56000 cells for the round edged blade and 69000 cells for the flat edged blade. Cells on the blade faces are clustered towards the edges to achieve a smooth transition from the blade edges to the blade faces. 6 cells were used to resolve the edges, which for a 0.5 mm thick blade results in a resolution of 0.13 mm for round edges and 0.08 mm for flat edges and a resolution of 0.026 mm and 0.017 mm respectively for a 0.1 mm thick blade. An o-grid surrounds the blade for the cells to be parallel to the blade surface. Inside the o-grid the cells are clustered towards the blade such that the boundary layer is resolved to an appropriate extent. The grid for the flat edged blade is shown in Fig. 6.

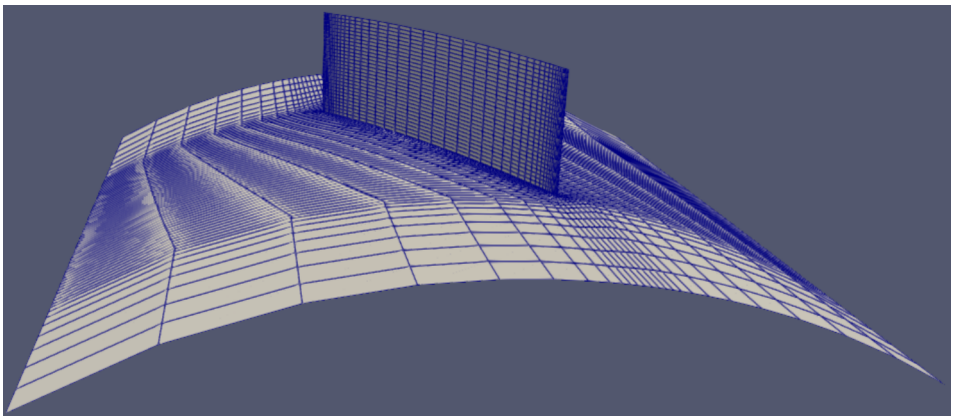

Fig 6. The computational grid for a 0.5 mm thick flat edged blade.

Figure 7 shows the results of a grid convergence study. The size of each cell was halved for every increase in spatial resolution. Shown is the error in power efficiency of three different grids relative to a

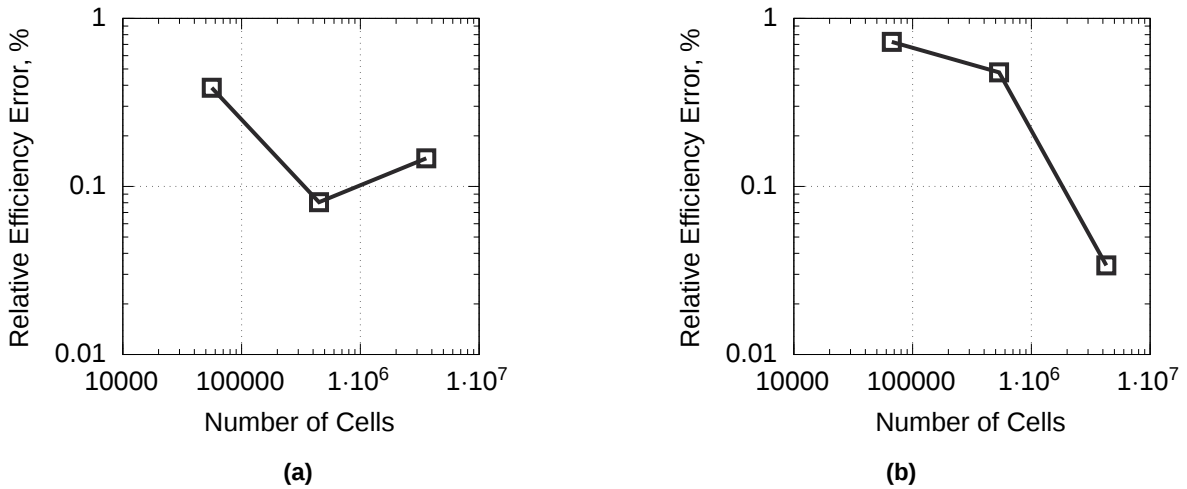

Fig 7. The error in efficiency relative to the largest grid for the blade with round edges (a) and the blade with flat edges (b).

grid with 28.0 million cells for the round edged blade and 34.2 million cells for the flat edged blade. The efficiency is chosen as a measure for convergence since it is of primary interest in this study. Considering

the magnitude of the error, the coarsest grid was used for this study. For the round edged blade, the error is not monotonically decreasing with an increase in the number of cells, however, the error is less than 1 % for each grid. The lack of monotonicity is likely due to the fact that the power efficiency is an integrated quantity. In general this could mean that neither of the grids appropriately resolve the flow. However, as Fig. 8 shows, the pressure contours are almost identical for all grids, the only significant differences appear at the edges. The shear stresses show significant differences but the

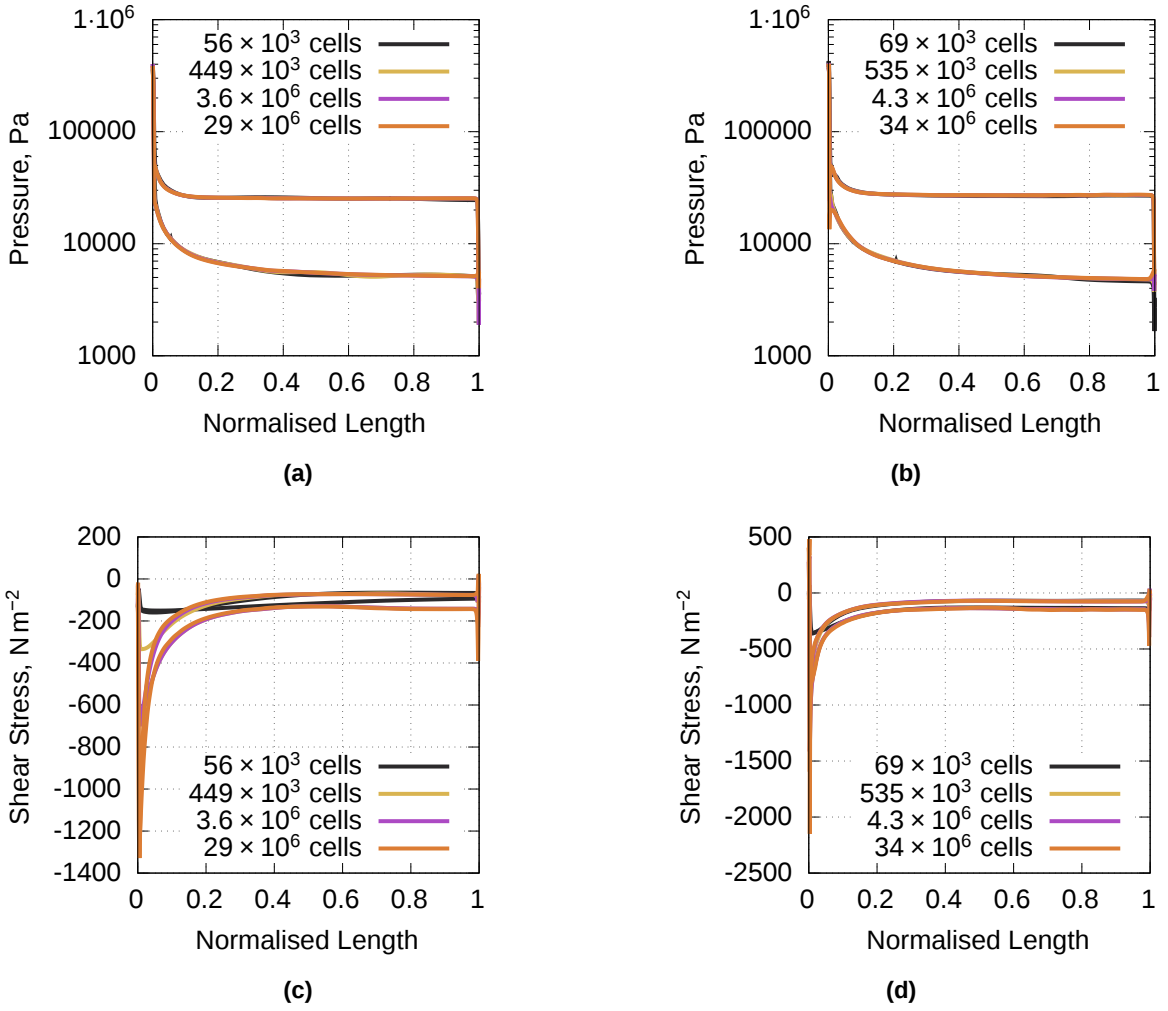

Fig 8. Pressure and shear stress contours on the round edged blade (a) and (c) and the flat edge blade (b) and (d) at $r = 0.19$ m.

magnitude of the viscous forces is so small that their effect on the power efficiency is negligible. Shown are the contours at $r = 0.19$ m, however, the differences are of a similar magnitude at any location on the blade. In Fig. 9 the progression of the power efficiency is shown over the simulated time. The graphs show that the simulations have reached steady state after about 0.25 ms for both edge types. The simulations presented in the following have, hence, been stopped at 0.25 ms. This is equivalent to 18.2 % of one rotation at the lower end of the rotational speed, i.e. 33000 rotations per minute, and 20.8 % of one rotation at the upper end, i.e. 50000 rotations per minute. At Mach 4 the flow, however, takes only 0.15 ms to traverse the computational domain and only 0.074 ms to traverse the blade. Therefore, 0.25 ms is enough time for the flow to reach steady state.

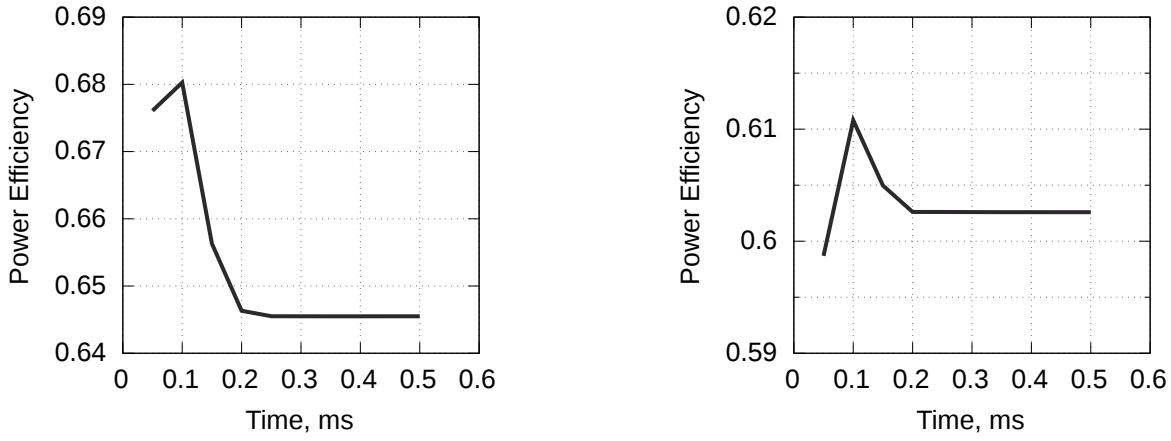

Fig 9. The temporal convergence for the blade with round edges (a) and the blade with flat edges (b).

3. Results

In this section, the results of the CFD simulations are shown and compared with the 2D results from Kunze and Paull [8]. Additionally, results from a quasi 3D calculation are shown. The quasi 3D model consists of a number of blade cross-sections at different radii, where the sum of the height of the cross-sections is equal to the total blade height. The equations are the same as in the 2D model, however, the quasi 3D model can take into account that the blade relative inflow varies with r. 10 cross-sections were used here. A further increase did not result in a noticeable change in efficiency.

Figure 10 shows the power efficiency of flat plate blades with different thicknesses compared to the 2D and quasi 3D results. Figure 10a shows round edged blades and 10b shows flat edged blades. The

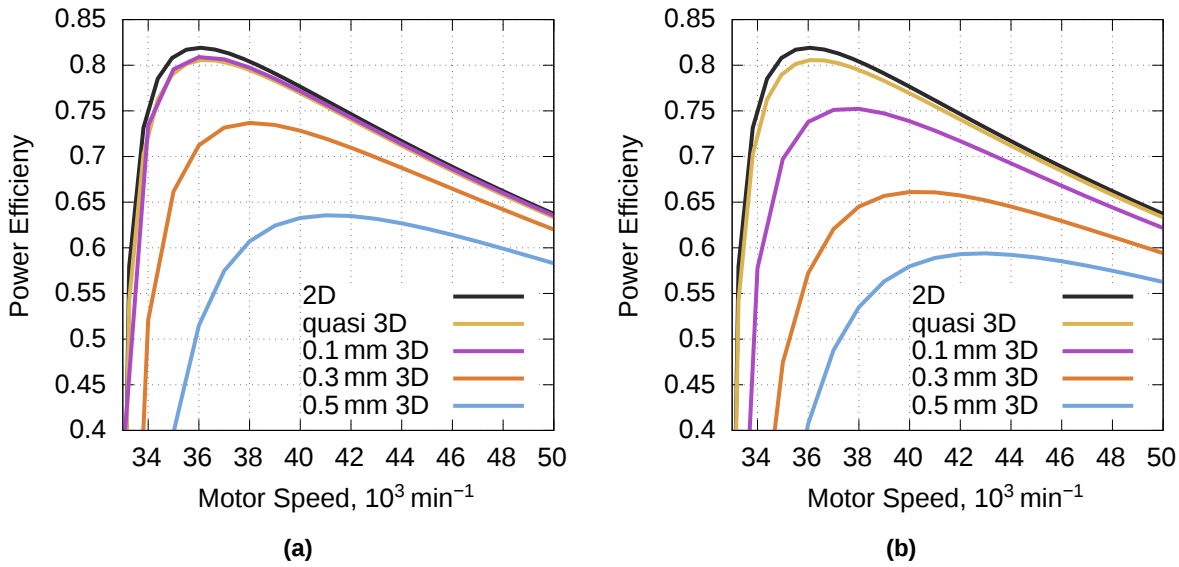

Fig 10. The power efficiencies of round edged blades blades (a) and flat edged blades with constant chord angles in comparison with 2D and quasi 3D results.

efficiency of the 0.1 mm thick blade with a round edge is about 2 % smaller than the prediction of the

2D model. However, the quasi 3D model agrees very well with the CFD result. With increasing blade thickness the agreement understandably gets worse. For the 0.5 mm thick blade the peak efficiency is 17 % below that of the quasi 3D blade and the peak shifts by about 5000 rotations per minute. Neither the 2D model nor the quasi 3D model make reasonable predictions for the performance of the flat edged blades. It appears that even for blades as thin as 0.1 mm the edge shape has a significant impact on the power efficiency, in this case a drop of over 5 %. Additionally, the efficiency peak shifts by about 2000 rotations per minute to a higher value which increases the demands on the motor. The main reason for the difference is that on a flat edge the maximum pressure is over five times higher than the maximum on a round edge. This means that the leading edge shock is stronger, resulting in higher losses. The pressure remains high on the entire flat edge, whereas on a round edge the average pressure is much lower than its peak. The flat edge is, furthermore, oriented such that its contribution to the thrust is disproportionately large compared to the blade faces, i.e. the angle between the axis of rotation and the surface normal of the flat edge is 30°, whereas the angle between the axis of rotation and the surface normal of the blade faces is 60°. The leading edge is, furthermore, contributing to the torque on the propeller, refer to Fig. 5. In total, the difference in thrust caused by the edge shape is about 8.5 %.

In Fig. 11 the quasi 3D and 3D blades are twisted such that the angle of attack is constant over the blade height at 2° angle of attack. As mentioned in section 2.1, the blade twist can not be modelled in 2D. The match between the quasi 3D model and CFD is again very good for the 0.1 mm thick round

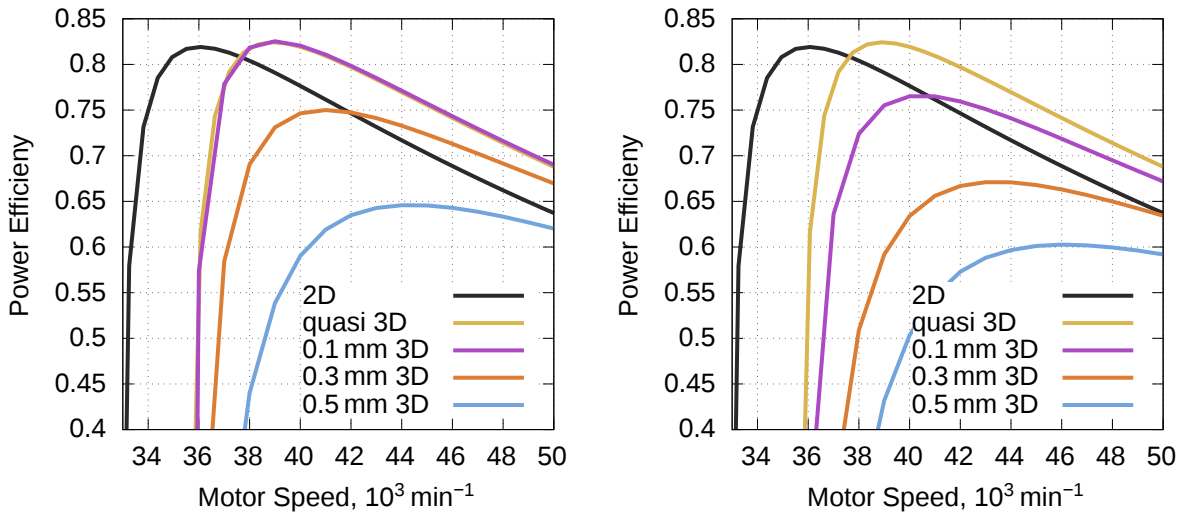

Fig 11. The power efficiencies of round edged blades blades (a) and flat edged blades with constant angles of attack at 2° angle of attack in comparison with 2D and quasi 3D results.

edged blade. The reduction in efficiency with an increase in blade thickness is of a similar magnitude as for the untwisted blade. As far as the magnitude of the power efficiency for the thin round edged blade is concerned, the 2D model still provides a very good prediction, albeit at a significantly lower rotational velocity. The discrepancy is due the blade twist. Although the angle of attack is only constant over the blade height at 2° angle of attack, there is much less of a variation in angle of attack compared to the untwisted blade. Hence, the twisted blade only start producing thrust once the rotational velocity at the blade root is high enough to result in a positive angle of attack. In the case of the untwisted blade, however, the angle of attack at the blade tip is positive at a much lower rotational velocity than the angle of attack at the blade root. For the blade to produce net thrust, the angle of attack has to be positive for more than half of the blade. The 2D model uses the flow conditions in the centre of the blade, i.e. at $r = 0.2$ m, which explains why the 2D model matches the power efficiency curve of the untwisted blade so closely. The curves for flat edged blades, again, do not align at all with either the 2D or the quasi 3D

model.

Figure 12 shows the power efficiency curves for two diamond shaped blades, calculated with the three different models, as well as the efficiency curve of the 2D flat plate for reference. The chord angle is constant for each of the blades and the edges are round with a radius of 0.05 mm. Even for a diamond

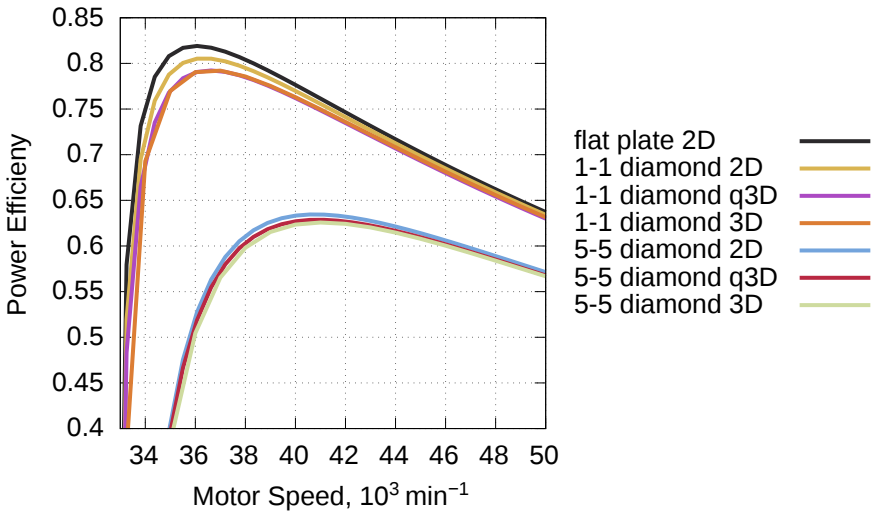

Fig 12. The power efficiencies of blades with a diamond cross-section.

shaped cross-section the agreement between the CFD results and the quasi 3D model is excellent. The agreement is better for the 1-1 diamond than the 5-5 diamond, however, the difference is marginal. Interestingly, the 2D model predicts the performance of the 5-5 diamond better than that of the 1-1 diamond.

4. Conclusions

The predictive capability of a 2D and a quasi 3D model for the performance of a supersonic propeller was studied. 3D CFD simulations in a rotating frame of reference were performed for this purpose. It was found that for edge radii of 0.05 mm and rounded edges, the CFD results matched very well with the results of the quasi 3D model for all blades. Even the 2D model provided a good estimate of the power efficiency. For larger edge radii the agreement reduced rapidly and the 2D and quasi 3D models over predicted the power efficiency of the blade significantly. Further work is required to study the effects of a blade tip, a viscous hub as well as more complex blade shapes. The 2D and quasi 3D models will need to be evaluated against those simulations as well, however, the results thus far show promise.

Funding

This research was collaboration between the Commonwealth of Australia (represented by the Defence Science and Technology Group) and the University of Queensland, through a Defence Science Partnerships agreement. Further funding was provided by MBDA UK Limited.

References

[1] IEA, “Tracking clean energy progress 2023,” 2023.

[2] S. Porter, P. Wellener, K. Hardin, and H. Ashton, “Electrification in industrials,” 2020.

[3] S. A. Sherrill, P. Banerjee, G. W. Rubloff, and S. B. Lee, “High to ultra-high power electrical energy storage,” *Physical Chemistry Chemical Physics*, vol. 13, no. 46, pp. 20714–20723, 2011.

[4] S. Shelar, “Groundwork for the development of a plasma fuelled engine,” mastersthesis, Centre for Hypersonics, School of Mechanical and Mining Engineering, The University of Queensland, 6 2021.

[5] R. M. Bass, “An historical review of propeller developments,” *The Aeronautical Journal*, vol. 87, pp. 255–267, 9 1983.

[6] J. Fabri and R. Siestrunck, “Study of the supersonic propeller,” Tech. Rep. NACA TM 1355, National Advisory Committee for Aeronautics, 3 1953.

[7] J. Winchester, *The World’s Worst Aircraft (From Pioneering Failures to Multimillion Dollar Disasters)*. Barnes & Noble Books, 3rd edition ed., 1 2005.

[8] J. Kunze and A. Paull, “Preliminary analysis of the performance of an electric supersonic propeller,” *Aerospace*, vol. 10, no. 9, p. 803, 2023.

[9] R. Seleznev, S. Surzhikov, and J. Shang, “A review of the scramjet experimental data base,” *Progress in Aerospace Sciences*, vol. 106, pp. 43–70, 4 2019.

[10] N. N. Gibbons, K. A. Damm, P. A. Jacobs, and R. J. Gollan, “Eilmer: An open-source multi-physics hypersonic flow solver,” *Computer Physics Communications*, vol. 282, p. 108551, 1 2023.

[11] C. Ventura, E. Sauret, P. Jacobs, P. Petrie-Repar, R. Gollan, and P. V. D. Laan, “Adaption and use of a compressible flow code for turbomachinery design,” in *Proceedings of the V European Conference on Computational Fluid Dynamics ECCOMAS CFD* (J. Pereira and A. Sequeira, eds.), pp. 1–3, Portugal: APMTAC/IDMEC, 2010.